Enhanced Thermo-Fluid Dynamic Modelling Methodologies for Convective Boiling

Tilak T. Chandratilleke and Nima Nadim

Abstract Analytical tools embedded in current thermal design practice for convective boiling systems are traditionally built upon correlated empirical data, which are constrained by the thermo-fluid dynamical complexities associated with stochastic and interactive behaviour of boiling fluid mixtures. These methodologies typically overlook or under-represent key characterising aspects of bubble growth dynamics, vapour/liquid momentum exchange, boiling fluid composition and local phase drag effects in boiling processes, making them inherently an imprecise science. Resulting predictive uncertainties in parametric estimations compromise the optimal design potential for convective boiling systems and contribute to operational instabilities, poor thermal effectiveness and resource wastage in these technologies. This book chapter first discusses the scientific evolution of current boiling analytical practice and predictive methodologies, with an overview of their technical limitations. Forming a foundation for advanced boiling design methodology, it then presents novel thermal and fluid dynamical enhancement strategies that improve modelling precision and realistic processes description. Supported by experimental validations, the applicability of the proposed strategies is ascertained for the entire convective boiling flow regime, which is currently not possible with existing methods. The energy-saving potential and thermal effectiveness underpinned by these modelling enhancements are appraised for their possible contributions towards a sustainable energy future.

Nomenclature

C_d	Drag coefficient
C_p	Specific heat (J/kg-K)
D_w	Bubble departure diameter (m)
E	Energy rate (W/m3)
f	Bubble departure frequency (Hz)

T.T. Chandratilleke (✉) · N. Nadim
Department of Mechanical Engineering, Curtin University, GPO Box U1987,
Perth, WA WA6845, Australia
e-mail: t.chandratilleke@curtin.edu.au

$\vec{F}_{lift}$	Lift force (N)
$\vec{F}^{TD}$	Turbulence drift force (N)
$\vec{F}_{wl}$	Wall lubrication force (N)
g	Gravity (m/s^2)
G	Mass flow rate (kg/s)
H	Enthalpy (kJ/kg)
h_{lg}	Latent heat (kJ/kg)
h_{sl}	Interfacial heat transfer coefficient (W/m^2-K)
Ja	Jacob number
k	Turbulent kinetic energy (m^2/s^2)
k_{eff}	Effective conductivity (W/m-K)
K_{pq}	Interfacial momentum transfer coefficient
L	Total length of the channel
L_H	Heated length of the channel
$\dot{m}$	Mass flux (kg/m^2-s)
p	Pressure (Pa)
$\dot{q}$	Heat flux (W/m^2)
r_c	Cavity radius (m)
T	Temperature (K)
u^*	Frictional velocity on the wall (m/s)
v	Velocity (m/s)
$\nabla\vec{V}$	Mean strain rate tensor
$\nabla\vec{V}^T$	Turbulent strain rate tensor
We_s	Surface Weber number
y^+	Dimensionless distance from wall
Y^*	Dimensionless vertical distance from centre of channel
Z^*	Dimensionless axial distance from channel inlet

Subscripts

b	Bubble
d	Droplet
b,d	Bubble or droplet
E	Evaporative
L	Liquid
m	Mixture
p	Primary phase
q	Secondary phase
Q	Quenching
Sat	Saturation
Sub	Subcooled
Sup	Superheated
v	Vapour
w	Wall

Greek Symbols

α Volume fraction
μ Viscosity (kg/m-s)
ρ Density (kg/m3)
σ Surface tension coefficient (n/m)
$\bar{\tau}$ Stress tensor
τ_D Bubble dwelling time (s)
τ_G Bubble growth time (s)
ω Specific dissipation rate (1/s)
λ Thermal diffusivity $(k/\rho c_p)$

1 Introduction

Owing to high thermal effectiveness associated with fluids undergoing phase change, convective flow boiling mechanisms are widely deployed in thermal energy conversion systems [1] such as steam power plants, industrial boilers, nuclear reactors, refrigerators and electronic cooling heat sinks. Thermal characteristics of flow boiling are crucial design considerations for such technological applications where the overall system performance is fundamentally governed by the dynamics of fluid phase change, flow structures developed and heat transport mechanisms within heated pipes carrying operating fluids. In these, vapour bubble generation and bubble detachment essentially influence the degree of flow turbulence and slip velocity between phases, which in turn determine the thermal and fluid flow characteristics.

Through decades of experimental work and numerical modelling, an extensive knowledge base has been developed in understanding the flow boiling regimes and thermal behaviour in straight pipes. As depicted in Fig. 1, a single phase fluid flow entering a heated pipe undergoes gradual phase change from Bubbly flow to the regimes of Slug, Annular and Mist flow along the pipe with increasing proportions of vapour volume or void fraction. These extreme changes in flow composition
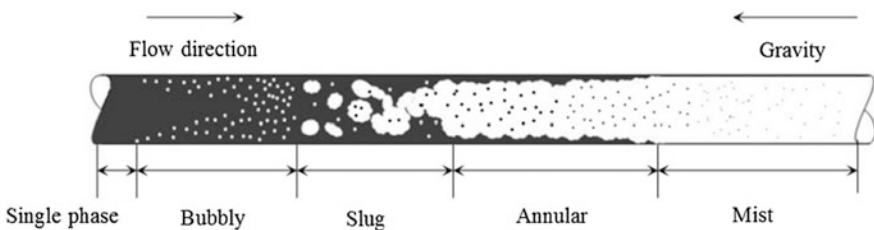

Fig. 1 Variation of flow regimes in upward convection boiling in a straight duct

create widely differing flow mechanisms within boiling regimes and would deter the development of unified thermal and flow simulation methodologies covering all boiling regimes.

The traditional modelling approach for two-phase involves the assumption of independent behaviour in fluid phases and treats the gas-liquid flow domain with slip velocity that contributes to augmented pressure loss. Thus, fluid pressure head losses and average heat transfer rates are computed for the cases of homogenous and non-homogenous mixtures. This approach evidently ignores the interfacial mass and momentum transfer between phases. Thermal and hydrodynamic behaviour in a boiling field has strongly inter-dependent mass and momentum transfers across phase interface due to condensation and/or evaporation processes present. Moreover, these dependencies significantly vary from bubbly flow regime to mist flow regime. Consequently, interfacial hydrodynamic models for gas-liquid systems are inadequate for accurate representation of convective boiling in pipes.

Among the models using gas-liquid interfacial concept, Lockhart and Martinelli [2] method is regarded the pioneering approach, where isothermal two-component flow is analysed for frictional pressure gradient. Another version by Martinelli and Nelson [3] addresses pressure drop during forced circulation boiling and condensation.

In improving accuracy and validity range of analytical solution, empirical and semi-empirical treatment of boiling fields have been suggested and utilised under various operating conditions and materials. Model and correlations suggested by Zuber et al. [4], Bankof [5], Marchaterre and Hoglund [6] and Griffith [7] have made significant contributions to the knowledge of multi-phase hydrodynamics in boiling. For more than five decades, those pioneering models have formed the traditional modelling basis in predicting key parameters of pressure loss, void fraction and slip ratio of phases whilst being the catalyst for further developments. However, heat transfer schemes deployed in traditional boiling analyses generally indicate large uncertainties towards the critical heat flux (CHF). This is due to the assumption of homogenous phase interaction in developing theoretical or empirical models. Moreover, simple mechanisms of fully developed nucleate boiling used would be inadequate for accurate representation of flow boiling phenomena.

For improved understanding of boiling processes, extensive parametric studies have been conducted to examine bubble nucleation, growth and detachment along with pipe wall dry-out, burnout and CHF. Bergles and Rohsenow [8] carried out an experiment observing the characteristics boiling curve for forced convection surface boiling with water at low pressure and investigated the bubble growth process and the requirements for onset of boiling. Comparison of these results indicated a marked difference to those of pool boiling characteristics. Extending his own correlation with large data sets and 10 test fluids, Kandlikar [9] developed a new correlation for boiling heat transfer in horizontal and vertical tubes. This correlation incorporating a fluid dependent parameter was shown to be valid for predicting both nucleate and convective boiling heat transfer. Analysing a uniformly heated coolant channel, Boyd and Meng [10] obtained heat transfer coefficients for both single phase and fully developed boiling (FBD) regimes. These authors suggested an

interpolation function to estimate the heat transfer coefficient for nucleate boiling conditions between the single phase and FBD regimes. However as a major drawback, these results were applicable only to the tested fluid in the study.

The next level of enhancement in boiling investigation was to explicitly investigate the dynamics of bubble behaviour at the wall and associated influence on thermal processes. Cole [11] concluded that bubble behaviour and growth at a heated surface are pivotal for accurate determination of heat and mass transfer, and boiling model development. Pioneering such research, Cole [11] conducted a photographic study of boiling phenomenon at heated surfaces up to CHF and identified three stages of dwelling, growth and departure associated with vapour bubble generation. He defined bubble departure frequency based on the fluid conditions and indicated its influence on bubble departure size. Although this study was performed under pool boiling conditions, his bubble departure frequency predictions were shown to provide an acceptable accuracy with flow boiling as well.

Thorncroft et al. [12] visually examined boiling characteristics for convective boiling under subcooled conditions in upward and downward channel flow. Considering heat and mass fluxes in the range of 13–14.6 kW/m^2 and 190–666 kg/m^{2}s, respectively, these authors reported significantly different bubble dynamics, where bubble sliding along nucleation sites was specifically observed. Bubbles were noted to grow partially attached to the nucleation site while most of the growth occurred during the sliding process. Their results were validated for different heat flux conditions by Situ et al. [13] in vertical annular flow using high-speed digital photography. This forced convection boiling analysis indicated bubble departure frequency was proportional to the wall heat flux and reported bubble lift-off diameter, bubble growth rate and bubble velocity after lift-off. In subsequent work, Situ et al. [14] formulated dimensionless form of bubble lift-off diameter as a function of Jacob and Prandtl numbers with acceptable consistency against the experimental data.

Basu et al. [15] have developed a subcooled flow boiling model by separating the wall heat flow into components at the pipe wall and formulated closures for bubble departure diameter, departure frequency, nucleation site density and surface properties. Model predictions were compared with the experimental tests performed for mass flow rates of 124–926 kg/m^2.s, heat fluxes of 25–900 kW/m^2 and contact angles of 30°–90°. These authors concluded that, when boiling approached fully developed conditions, the wall heat transfer was dominated by the transient heat conduction in the superheated liquid film at the wall and consequently, the flow velocity had less influence on the overall heat transfer rate. Compared to other analyses, this model accounted for bubble sliding effect in determining bubble dynamics although the requirement of contact angle value was a major drawback.

Describing bubble ebullition cycle in subcooled convective boiling, Podowski et al. [16] proposed a mechanistic model based on one-dimensional transient heat transfer from pipe wall surface to bubble while accounting for dwelling and growth of bubbles. These authors considered a comprehensive set of parameters such as subcooled temperature, bubble departure diameter, transient heat flux, wall

characteristics (material properties and cavity radius), making the model one of the most trusted for predicting bubble departure frequency in subcooled convective boiling.

Situ et al. [17] obtained an extensive experimental dataset which indicated fundamentally different bubble behaviour under pool and convective boiling conditions. This provided an important basis for grouping of boiling models according to bubble behaviour. For instance, as boiling regime approaches to a pool boiling case, where bubble detachment process is purely controlled by buoyancy force, bubble shape, density number, and critical diameter are significantly different from convective boiling. On the other hand, in presence of shear flows, in convective boiling, new phenomena should be accounted such as bubble deformation, bubble sliding on the wall and more complicated detachment process.

Advances in boiling knowledge, inclusive of bubble dynamics, phase interaction and phase transition, have warranted the development of many numerical simulation models that would overcome limitations of traditional approaches and extend analytical capabilities into deeper examination of boiling regimes.

Forming the basis for majority of published numerical models, Kurul and Podowski [18] first presented the wall heat partitioning concept as a key technique for developing boiling closure. At the forefront of this is the RPI (Rensselaer Polytechnic Institute) model of which the wall heat flux is taken to be contributed by three components of heat transfer through liquid, that due to quenching and liquid evaporation. The model also assumes thermal equilibrium between the phases of vapour and liquid, therefore the vapour is treated to be fixed at saturation temperature.

For several decades, the RPI model, which is a Eulerian two-phase approach, has been applied for various boiling cases with attempts to modify and validate it. Koncar et al. [19] utilised the simplest form of RPI, with three heat partitioning components and pool boiling bubble departure frequency. This study investigated local subcooled flow boiling at low pressure and demonstrated the model validity for maximum void fraction of 0.3. For analysing a fuel assembly design, Krepper et al. [20] modified the RPI model by introducing a correction for liquid wall temperature to be mesh-independent and based on liquid temperature at a fixed y^+ value. Koncar and Krepper [21] used the RPI model through CFX commercial CFD package for investigating boiling of R-113 in a vertical annulus. These authors reported a good agreement with experimental measurements. For a parametric investigation of subcooled jet impingement boiling, Abishek et al. [22], obtained satisfactory outcomes for isothermal and isoflux jet impingement boiling that were validated against test data.

Review of current literature identifies limitations of published boiling simulation models with possibilities for improvements. In these, the closures for bubble dynamics are typically estimated through pool boiling data ignoring the significance of surface characteristics, varying nature of bulk flow within regimes and the influence of flow shear on vapour bubbles. Addressing these limitations, this book chapter demonstrates feasible enhancements to convective boiling models for better representation of flow intricacies over the entire range of flow boiling regimes,

where the void fraction varies from low values in the bubbly region to high magnitudes in the mist flow regime. Based on Eulerian multi-phase framework, the proposed model incorporates a mechanistic description for bubble dynamics accounting for surface properties (wall material properties and temperature) and bulk flow velocity. It also includes an enhanced momentum exchange scheme for accurate estimation of slip velocity between phases that undergo extreme variations with slug and mist flow conditions. For ascertaining the effectiveness of the modified closures, well-established experimental data for subcooled flow boiling within rectangular ducts by Pierre and Bankoff [23] are used as the evaluation benchmark. The model is validated with not one, but both void fraction and phase slip velocity to ensure accuracy and conformity through overall and interfacial mass exchange rates. The paper also provides, as a guide, a description of essential modelling elements to be considered for improved convective boiling simulations. It is viewed that these modelling enhancements will improve and consolidate the current convective boiling design practice, leading to better thermal efficiency, energy saving and resource utilisation in boiling systems, hence contributing to a sustainable energy future.

2   Development of Computational Framework

The model developed and presented in this book chapter paper uses the following governing equations with Eulerian approach where the liquid and vapour phases are separately considered in solving the momentum, mass and energy conservation equations. The turbulence equations is solved for mixture (defined according to mixture velocity and material properties) while pressure is shared between both phases. In writing these equations, liquid and vapour phases are denoted by subscripts "p" and "q", respectively.

(a) Mass, momentum and energy conservation

The continuity equations are written as (only phase "q" is show to prevent repetition),

$$\nabla.(\alpha_q \rho_q \vec{v}_q) = \dot{m}_{qp} - \dot{m}_{pq} \tag{1}$$

The momentum conservation equations, which are coupled by mass transfer, momentum exchange coefficient and other interfacial forces, are defined as (only phase "q" is show to avoid repetition),

$$\nabla(\alpha_q \rho_q \vec{v}_q \vec{v}_q) = -\alpha_q \nabla p + \nabla.\bar{\bar{\tau}}_q + \alpha_q \rho_q \vec{g} + K_{pq}(\vec{v}_p - \vec{v}_q) + \dot{m}_{pq}\vec{v}_{pq} - \dot{m}_{qp}\vec{v}_{qp}$$
$$+ \vec{F}_q^{TD} + \vec{F}_{wl} + \vec{F}_{lift} \tag{2}$$

Stress tensor of each phase accounting for the effects from molecular and turbulence viscosity is written as (only phase "q" is show to prevent repetition),

$$\bar{\bar{\tau}}_q = \alpha_q \mu_q \left(\nabla \vec{v}_q + \nabla \vec{v}_q^T \right) + \alpha_q \left(\lambda_q - \frac{2}{3} \mu_q \right) \nabla . \vec{v}_q \bar{\bar{I}} \tag{3}$$

Energy conservation equation for liquid/vapour mixture is given by,

$$\nabla(\alpha_q \rho_q \vec{v}_q H_q) = -\alpha_q k_q \nabla T_q + Q_{pq} + \dot{m}_{pq} H_{pq} - \dot{m}_{qp} H_{qp} \tag{4.a}$$

and mixture scalars are calculated as,

$$\rho_m = \alpha_l \rho_l + \alpha_v \rho_v \text{ and } \vec{v}_m = \frac{\alpha_l \rho_l \vec{v}_l + \alpha_v \rho_v \vec{v}_v}{\alpha_l \rho_l + \alpha_v \rho_v}, E = \frac{\alpha_l \rho_l E_l + \alpha_v \rho_v E_v}{\alpha_l \rho_l + \alpha_v \rho_v} \tag{4.b}$$

(b) Turbulence

Using k-ω SST turbulence model, transport equations will be shared for liquid/vapour mixture (i.e. using mixture velocity and material properties for each phase) as follows,

$$\nabla . (\rho_m k_m \vec{v}_m) = \nabla . \left((\mu + \frac{\mu_t}{\sigma_k}) \nabla k_m \right) + G_k - Y_k \tag{5.a}$$

$$\nabla . (\rho_m \omega_m \vec{v}_m) = \nabla . \left((\mu + \frac{\mu_t}{\sigma_\omega}) \nabla \omega_m \right) + G_\omega - Y_\omega \tag{5.b}$$

In this, $G_{k,\omega}$ and $Y_{k,\omega}$, which are generation and dissipation rate term for k and ω, have the common formulation for standard and SST version of k-ω closure [24, 25], whereas σ_k and σ_ω (k and ω Prandtl number) are specifically derived for SST version of k-omega model by Mentor [24]. Turbulence induced by the presence of bubbles/droplets as dispersed phase has to be accounted for in the closure when used in a multi-phase frame. In taking this into consideration, various methodologies propose either explicit source terms to be included in transport turbulence equation [26] or alternatively, suggest modifying turbulence viscosity incorporating random primary phase motion originated by dispersed phase [27]. Following Sato et al. [28], the current model uses turbulent viscosity modification for dispersed phase as,

$$\mu_{td} = C_{\mu d} \rho_m \alpha_v d_{b,d} |\vec{v}_v - \vec{v}_l| \tag{6}$$

where $C_{\mu d}$ is an adjustable coefficient in the range of [0.5, 0.75]. For the analysis, $C_{\mu d}$ is chosen as 0.65, which is an estimation for density ratio $\left(\frac{\rho_l}{\rho_v} \right)$ range of (25, 130). This source term may be applied to various regimes by assuming particle

as bubbles (d_b) or droplet (d_p). Then for the liquid/vapour mixture, total turbulence viscosity is formulated as,

$$\mu_{tm} = \frac{\rho k}{\omega} \frac{1}{\max\left[\frac{1}{\alpha^*}, \frac{SF_2}{\alpha_1 \omega}\right]} + \mu_{td} \tag{7}$$

where S is the mean rate of strain tensor while the coefficient α^* dampens turbulent viscosity if low-Reynolds correction is applied with F_2 and α_1, which are part of functions proposed in the SST closure. Since all the interfacial exchange terms are interpreted as a source term in the primary (continuous) phase, in turbulence equations, solving k and ω equations for the mixture or separately in phases is not anticipated to make a noticeable difference. Besides, turbulence dispersion is independently accounted as a source term in the momentum equation while the turbulence agitation effect from dispersed phase (turbulence interaction) is included in RANS equations separately. In implementing the turbulence equation in the mixture domain, the turbulence controlling parameters are monitored with respect to the mixture phase parameters, for example y$^+$ through $y_m^+ = \frac{\rho_m u_m^* y_{wall\_cell}}{\mu_m}$. This approach is confirmed by comparing results from the trial runs having mixture versus per-phase schemes that give identical results. Therefore, the mixture scheme is applied to enhance numerical stability and reduce computational effort whilst achieving the same level of turbulence resolutions.

(c) Wall heat partitioning

Current flow boiling simulation is developed as a non-equilibrium model alleviating a major modelling drawback in the RPI approach, where thermal equilibrium is assumed between liquid and vapour phases. It considers three wall heat partitioning components, namely the liquid convective, quenching and evaporative heat fluxes as with the RPI approach. In addition, it also includes a fourth heat partitioning component to account for diffusive heat flux within bubble vapour phase, hence removing the RPI assumption of vapour being in equilibrium at saturation temperature. Contribution from the forth heat partitioning term is particularly important for convective boiling with large void fraction and improves the applicability of analysis.

Summing up the four heat flux contributions, the total wall heat flux is obtained to be,

$$\dot{q}_{Total} = (\dot{q}_L + \dot{q}_Q + \dot{q}_E)f(\alpha) + \dot{q}_V(1 - f(\alpha)) \tag{8}$$

where $f(\alpha)$ is a function which is defined according to the phase distribution and the flow regime. Following Lavieville et al. [29], the current model uses the expression given below,

$$f(\alpha) = \begin{cases} 1 - \frac{1}{2}\exp(-20(\alpha_l - 0.2)) & \alpha_l \geq 0.2 \\ \frac{1}{2}\left(\frac{\alpha_l}{0.2}\right)^4 & \alpha_l < 0.2 \end{cases} \tag{9}$$

Known as boiling closure, Eq. (10.a, 10.b) below provides the diffusive heat component for each phase during boiling/condensation processes. In this, $\dot{q}_L$ and $\dot{q}_V$ are convective terms calculated for liquid and vapour phases using temperature gradient at wall, their area of influence and local fluid properties.

$$\dot{q}_L = h_L(T_W - T_L)(1 - A_b) \tag{10.a}$$

$$\dot{q}_V = h_V(T_W - T_V) \tag{10.b}$$

Convective liquid and vapour heat transfer coefficients (h_L, h_V) are computed from the wall function formulations in a RANS framework.

In Eq. (10.a, 10.b), A_b is the area covered by bubble and is calculated based on bubble departure diameter and an empirical constant K ranged between 1.8 and 5. These parameters are estimated following the suggestions by Del Valle and Kenning [30] from,

$$A_b = K\frac{N_w \pi D_w^2}{4} \tag{11.a}$$

$$K = 4.8 \exp(-\frac{Ja_{sub}}{80}) \tag{11.b}$$

where N_w is nucleation site density. N_w is obtained from the empirical expression of Lemmert and Chawala [31] as,

$$N_w = 210^{1.805}(T_w - T_{Sat})^{1.805} \tag{12}$$

while the Bubble departure diameter (D_w) is computed from the semi-empirical correlation developed by Tolubinski and Kostanchuk [32],

$$D_w = \min(0.0014, 0.0006 \exp(-\frac{\Delta T_{Sub}}{45}) \tag{13}$$

where local subcooling is defined as $\Delta T_{Sub} = T_{Sat} - T_{bulk}$

In Eq. (8), $\dot{q}_Q$ and $\dot{q}_E$ are cyclic-averaged heat transfer rates for quenching (i.e. heat removal by liquid re-entering the wall region after bubble detachment) and evaporation (i.e. latent heat) processes. These heat transfer rates are evaluated over one cycle period of bubbles defined as the time difference between two consecutive bubble departures. Based on experimental observations, one cycle period is taken to comprise of bubble dwelling (or waiting) phase and bubble growth phase [11, 15, 16]. Following Podowski model, the dwelling and growth times are calculated for the

present model to estimate the bubble departure frequency. In this, bubble dwelling time is given by,

$$\tau_D = \left[(-C_2 + \sqrt{C_2^2 - 4C_1 C_3})/2C_1\right]^2 \tag{14.a}$$

where

$$C_1 = \frac{2q_w''}{\Re \pi} \tag{14.b}$$

$$C_2 = (\frac{k_w T_w}{\sqrt{\lambda_w}} + \frac{k_l T_{bulk}}{\sqrt{\lambda_l}})/(\frac{k_w}{\sqrt{\lambda_w}} + \frac{k_l}{\sqrt{\lambda_l}}) - T_{sat} - \frac{q_w'' r_c}{\Re \sqrt{\pi \lambda_l}} \frac{r_c}{r_c} - \frac{2\sigma}{r_c} \frac{T_{sat}(\alpha_v/\rho_v - \alpha_l/\rho_l)}{h_{lv}} \tag{14.c}$$

$$C_3 = -\left[(\frac{k_w T_w}{\sqrt{\lambda_w}} + \frac{k_l T_{bulk}}{\sqrt{\lambda_l}})/(\frac{k_w}{\sqrt{\lambda_w}} + \frac{k_l}{\sqrt{\lambda_l}}) - T_b\right] \frac{r_c}{\sqrt{\pi \lambda_l}} \tag{14.d}$$

and

$$\Re = \frac{k_w}{\sqrt{\pi \lambda_w}} + \frac{k_l}{\sqrt{\pi \lambda_l}} \tag{15}$$

while the bubble growth time is given by,

$$\tau_G = \left[(-A_2 + \sqrt{A_2^2 - 4A_1 A_3})/2A_1\right]^2 \tag{16.a}$$

where

$$A_1 = \frac{q_w''}{k_w} \tag{16.b}$$

$$A_2 = 2[(\frac{k_w T_w}{\sqrt{\lambda_w}} + \frac{k_l T_b}{\sqrt{\lambda_l}})/(\frac{k_w}{\sqrt{\lambda_w}} + \frac{k_l}{\sqrt{\lambda_l}}) + \frac{2q_w'' \sqrt{\tau_D}}{\Re \pi} - T_{sat}]/\sqrt{\pi \lambda_w} \tag{16.c}$$

$$A_3 = \frac{D_w \rho_g h_{lv}}{2k_w} \tag{16.d}$$

Explained formulations for dwelling and growth times are derived by coupling transient heat transfer solutions for the heated wall and for the liquid filling the space vacated by departing bubbles. This approach is later discussed and compared against Cole model, which accounts solely for buoyancy force, in detachment process.

The bubble departure frequency is then obtained as,

$$f_{Departure} = \frac{1}{\tau_{B-Cycle}} = \frac{1}{\tau_D + \tau_G} \tag{17}$$

Hence, quenching and evaporation heat fluxes are computed from,

$$\dot{q}_Q = \frac{2k_l}{\sqrt{\pi \lambda_l \tau_{B-Cycle}}}(T_w - T_l) \tag{18.a}$$

$$\dot{q}_E = \frac{\pi D_w^3}{8} N_w \rho_v h_{lg} \tag{18.b}$$

The formulation explained through Eqs. (8–18.a, 18.b) outlines the scheme used for heat partitioning during flow boiling. The section below describes the processes at the liquid-vapour interface.

(d) Interfacial exchange properties

Eulerian framework is fundamentally based on analysis with designated continuous/dispersed phases within a flow regime. Almost all published Eulerian boiling models [18–21] have been developed with the assumption of bubbly flow to comply with low void fraction for which liquid is designated as continuous phase and vapour as dispersed phase. This assumption breaks down for large void fractions such as flow boiling in the mist regime, wherein liquid (droplets) becomes the dispersed particle in continuous vapour phase. Therefore, all published flow boiling models lack the ability to capture flow characteristics over the entire boiling regime and are limited in applicability. This drawback is effectively overcome in the current model with a smoothing function for interfacial parameters defined by,

$$\Phi = (1 - f(\alpha))\Phi_{Bubbly} + f(\alpha)\Phi_{mist} \tag{19}$$

where Φ is any exchange parameter dependant on local cell-base volume fraction and flow regime.

In applying Eq. (19), bubbly regime is defined as vapour volume fraction $\alpha_v \leq 0.4$ wherein vapour bubble is treated as dispersed phase in continuous liquid phase. For intermediate volume fraction of $0.4 < \alpha_v \leq 0.8$, liquid is taken to be primary phase with vapour as secondary phase. In here, drag force coefficient is modified according to churn turbulent regime formulation. If vapour volume fraction $\alpha_v > 0.8$, mist regime is assigned with liquid droplets as dispersed phase within continuous vapour phase [25, 33]. Based on such a framework, interfacial exchange values and applied closure are briefly explained as follows:

(e) Bubble and droplet diameter

Following a formulation by Unal [34], the bubble diameter is expressed as a function of local subcooling temperature as,

$$D_b = \begin{cases} 0.0015 & \Delta T_{Sub} < 0 \\ 0.00015 - 0.0001\Delta T_{Sat} & 0 < \Delta T_{Sub} < 13.5 \\ 0.00015 & \Delta T_{Sub} > 13.5 \end{cases} \qquad (20)$$

However, in the mist flow regime, where liquid droplets constitute dispersed phase, the droplet diameter is estimated using the correlation suggested by Kotaoka et al. [35] as,

$$D_d = 0.028 \frac{\sigma}{\rho_v V_v^2} \mathrm{Re}_l^{-1/6} \mathrm{Re}_v^{2/3} \left(\frac{\rho_v}{\rho_l}\right)^{-1/3} \left(\frac{\mu_v}{\mu_l}\right)^{2/3} \qquad (21)$$

where Re_l and Re_v are liquid and vapour Reynolds number, respectively. These correlations have been proven to be successful in many published boiling investigations.

(f) Momentum exchange coefficient and drag force

As a key parameter in Eulerian approach, it is required to define momentum exchange coefficient (K_{pq}) that determines slip velocity between phases, which in turn significantly influence other interfacial parameters such as mass transfer and void fraction. This exchange coefficient in Eulerian scheme is defined as,

$$K_{pq} = -K_{qp} = \frac{\rho f_D}{6\tau_p} D_p A_i \qquad (22)$$

where, subscript "p" denotes dispersed phase which could be bubble or droplet depending on the flow regime. A_i is the interfacial area, and f_D is drag function defined according to drag coefficient. In the drag function, the particulate relaxation time τ_p is given by,

$$\tau_p = \frac{\rho_p D_p^2}{18\mu_q} \qquad (23)$$

Ishii and Zuber [36] have provided a comprehensive drag coefficient and slip velocity functions for liquid-gas flows. These authors provided different correlations to estimate drag function for a wide range of flow regimes including bubbly, mist and churn turbulent regimes, similar to flow regimes adopted for the current model. Both bubbly and mist flow regions are assumed to have continuous-dispersed drag coefficient where viscosity ratio of phases would decide on the appropriate correlation. From Ishii-Zuber, drag coefficient is expressed for the three regimes as,

$$C_D = \begin{cases} \frac{4}{6} D_b \sqrt{\frac{g \Delta \rho}{\sigma}} (1 - \alpha_v)^{-0.5} & bubbly \quad regime \\ \frac{8}{3} (1 - \alpha_v)^2 & Churn \quad turbulent \quad regime \\ \frac{4}{6} D_d \sqrt{\frac{g \Delta \rho}{\sigma}} (1 - \alpha_l)^{-1.5} & mist \quad regime \end{cases} \quad (24)$$

This use of applicable drag coefficient for each flow regime is one of the key improvements in the current model compared to previously published work, where such models indiscriminately assigned a single drag coefficient and assumed continuous liquid phase and dispersed vapour bubbles over the entire computational domain. The drag function in Eq. (22) is then computed with the drag coefficient applicable for a particular regime from Eq. (23) using,

$$f_d = \frac{C_D \mathrm{Re}_{lv}}{24} \quad (25)$$

Relative Reynolds number $\mathrm{Re}_{lv} = \frac{\rho |v_l - v_v| D_p}{\mu}$ in Eq. (25) is computed by using continuous phase density, viscosity and dispersed phase particle sizes.

(g) Lift force

Correlation developed by Morega et al. [37] has been examined for various flow conditions and geometries. It is reported to have reasonable consistency for estimating interfacial lift force in nucleate boiling regime. This, bubbly flow, is formulated in the current model as,

$$\vec{F}_{lift} = C_{lift} \rho_l \alpha_v (\vec{v}_v - \vec{v}_l) \times (\nabla \times \vec{v}_l) \quad (26.a)$$

and

$$C_{lift} = \begin{cases} 0.0767 & \varphi \leq 6 \times 10^3 \\ \left[0.12 - 0.2 \exp(-\frac{\varphi}{36000}) \right] \exp(\varphi / 3 \times 10^7) & 6 \times 10^3 \leq \varphi \leq 1.9 \times 10^5 \\ 0.002 & \varphi \geq 1.9 \times 10^5 \end{cases}$$

$$(26.b)$$

where $\varphi = \mathrm{Re}_B \mathrm{Re}_\nabla$. For Eq. (26.a, 26.b), the bubble Reynolds number and bubble shear Reynolds numbers are respectively defined as $\mathrm{Re}_B = D_b \rho_l |v_l - v_v| / \mu_l$ and $\mathrm{Re}_\nabla = D_b^2 \rho_l |\nabla \times \vec{v}_l| / \mu_l$.

In the mist flow, however, lift force will be applied from continuous vapour phase to dispersed droplets and lift coefficient (C_{lift}) will be obtained using droplet Reynolds number ($\mathrm{Re}_d = D_d \rho_v |v_l - v_v| / \mu_v$) and droplet shear Reynolds number $\left(\mathrm{Re}_\nabla = D_d^2 \rho_v |\nabla \times \vec{v}_v| / \mu_v \right)$.

(h) Turbulence dissipation force

This interfacial parameter influences the process of vapour transportation from wall to core area of flow. Following a formulation by Lopez de Bertodano [38], turbulence dissipation force is evaluated from,

$$\vec{F}_{pq}^{TD} = C_{TD}\rho_l k \nabla \alpha_v \tag{27}$$

where C_{TD} is taken to be 1 although it could be calibrated for a certain case.

(i) Wall lubrication force

In many boiling experiments, the maximum void fraction is reported to occur near the wall separated by a liquid layer. This imparts a force called wall lubrication force on the secondary (vapour) phase. In the current model, this is accounted for by the formulation,

$$\vec{F}_{wl} = C_{wl}\rho_l \alpha_v \left| (\vec{v}_v - \vec{v}_l)_{||} \right|^2 \vec{n}_w \tag{28}$$

where $\left| (\vec{v}_v - \vec{v}_l)_{||} \right|$ is the relative velocity component tangential to wall and $\vec{n}_w$ is the unit normal vector on the wall. Among various correlations suggested, this analysis uses the correlation for C_{wl} by Hosokawa et al. [39],

$$C_{wl} = \max\left(\frac{7}{\text{Re}_B^{1.9}}, 0.021 \frac{g\Delta\rho D_B^2}{\sigma} \right) \tag{29}$$

(j) Interfacial heat transfer and mass transfer

When vapour bubbles depart the wall, the heat transfer from vapour bubble to liquid phase is given by,

$$\dot{q}_{lt} = A_i h_{sl}(T_{sat} - T_l) \tag{30}$$

where the heat transfer coefficient h_{sl} is calculated from the correlation suggested by Ranz–Marshal [40] as,

$$h_{sl} = \frac{k_l}{D_b}(2 + 0.6\text{Re}^{0.5}\,\text{Pr}^{0.33}) \tag{31}$$

Additionally, the vapour interfacial heat transfer (or heat transfer from super-heated liquid to vapour) is given by,

$$\dot{q}_{vt} = \frac{\alpha_v \rho_v c_{pv}}{0.05}(T_{sat} - T_v) \tag{32}$$

The bubble/droplet interfacial mass transfer is calculated from,

$$\dot{m}_i = \dot{m}_{lt} + \dot{m}_{lv} = \frac{\dot{q}_{lt} + \dot{q}_{vt}}{h_{fv}} \tag{33}$$

Interfacial formulation in Eqs. (27–32) is represented considering bubbly flow regime where bubbles are dispersed in continuous liquid phase. When applying these equations for mist flow regime, dispersed and continuous phases are interchanged to account for dispersed liquid droplets in vapour phase.

All the equations, accounting for interaction between particle and continuous phase, in the core area of flow, include particle characteristics (e.g. diameter, velocity). Particle characteristics, in these equations, are defined with reference of disperses phase which could be either bubble or droplet. Nevertheless, boiling closures, which accounts for bubble nucleation process and restricted to nucleation sites on the heated surface [Eqs. (11.a, 11.b–18.a, 18.b) and (27–33)], are applied merely with reference to droplet characteristics even in high volume fraction.

## 3 Model Evaluation and Application

(i) Numerical validation

For ascertaining the validity of the model developed and its hydro-thermal assumptions, the numerical predictions are compared with the experimental work of Pierre and Bankof [23] using the original ANL report [41]. In this, comparisons were carried out for both transverse and axial variations of void fraction throughout the channel to ascertain the predictive accuracy of phase patterns. The agreement of phases and slip velocity were additionally evaluated, and are presented later in the text where the enhancement of drag scheme is discussed.

Pierre and Bankof [23] experiments investigated flow boiling in vertically mounted straight stainless steel rectangular heated ducts with water flowing upward against gravity. The ducts were 1550 mm long with cross sectional dimensions of 44.45 mm × 11.5 mm and 0.43 mm wall thickness. The ducts were heated over a length of 1257 mm from inlet by passing electrical current through the duct walls. Ducts were provided with 13 test windows where γ-attenuation technique was installed. Using 0.8 mm collimator windows, the authors measured the transverse radially averaged void fraction over 11 mm width of chosen cross sections for volumetric flow rates.

The development of vapour phase is first examined in the axial direction, where the experimental void fraction is available as averaged values on successive cross sections located at dimensionless distance ($Z^* = z/L$) from the duct inlet. As such, numerically predicted void fraction is radially averaged at each plane (A to M) and plotted against the corresponding experimental values [27], as illustrated in Fig. 2.

Fig. 2 Development of axial void fraction
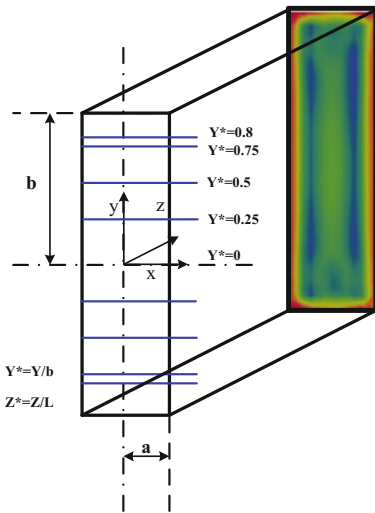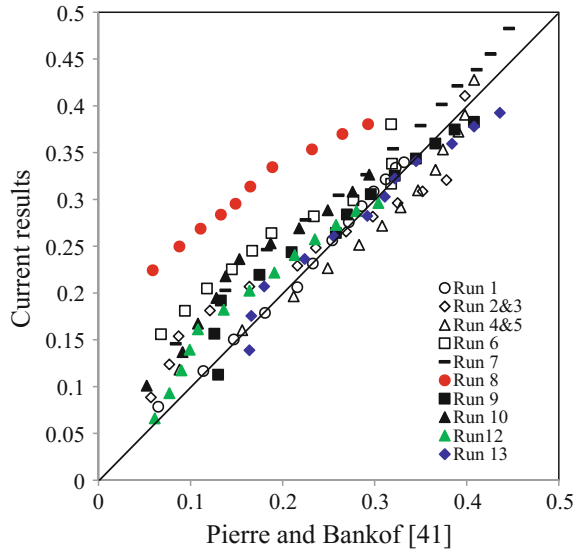
(a) Transverse profiles
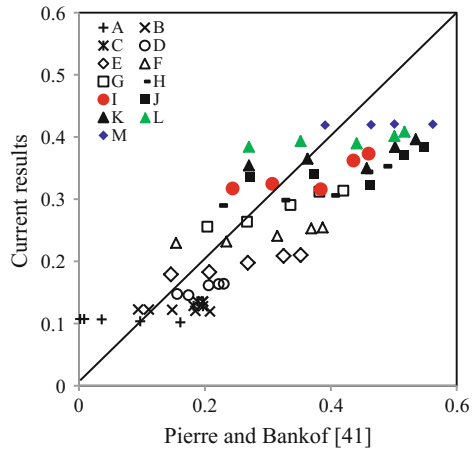
(b) Run 7

Fig. 3 Comparison of transversely averaged void fraction for different cross sections (A—M)

Considering the narrow scatter band and possible experimental uncertainties, this comparison is regarded as a very good agreement.

As an extended test of validation, transverse measurements of phase patterns are also compared in Fig. 3. Figure 3a shows five lateral profiles (Y* = y/b = 0 to 0.8),

where transverse void fraction is experimentally measured for each cross sections at A to M ($Z^* = 0.104$ to 0.831). Figure 3b illustrates the comparison of the numerically predicted transverse profile for these cross sections with the corresponding experimental data [23]. A very good agreement is again clearly evident from this comparison (Table 1).

(ii) Model Setup

Within FLUENT commercial CFD code, full three-dimensional duct geometry is implemented using finite-volume solver with non-equilibrium heat partitioning scheme. Default submodels were modified, as explained in sections describing computational framework, to include User Defined Functions (UDF) to incorporate drag coefficients, bubble departure frequency, quenching corrections and bulk temperature estimation. Saturation properties of water were extracted from the database of National Institute of Standards and Technology [42] for operating pressures, as provided in Table 2. Coupled and modified HRIC (high-resolution interface capturing) schemes were applied, respectively for pressure-velocity coupling and volume fraction discretization method with flow Courant number ranging between 5–10 depending on stability and convergence conditions. In ensuring reliability of convergence, in addition to essential checking of continuity and energy convergence over the entire domain, total mass and heat balance over the computational domain were also monitored.

Dimensions of flow passage geometry are obtained from duct in the Pierre and Bankof experiment (i.e. cross section of 11.5×44.45 mm, 1550 mm total length). A fully hexagonal mesh was considered with a sensitivity analysis that was carried out for mixture velocity, volume fraction and temperature with less than 0.5% variation allowance. Accordingly, a minimum mesh size of $0.5 \times 0.5 \times 0.8$ mm was used in core flow area which ends up with maximum cell number of 4566,003.

Table 1 Experimental operating conditions and test results by Pierre and Bankof [23, 41]

	Pressure (atm)	Inlet Velocity (m/s)	Average Heat flux (kW/m^2)	Inlet Subcooling	Saturation Temperature (K)
Run 1	13.61	1.15	71.88	0.28	466.86
Run 2 and 3	20.41	0.77	71.88	1	487.22
Run 4 and 5	27.21	0.77	143.75	2.67	502.37
Run 6	27.21	0.77	143.75	5.28	502.37
Run 7	27.21	1.15	215.63	0.67	502.37
Run 8	27.21	1.15	215.63	4.5	502.37
Run 9	40.82	1.15	287.51	2.33	524.7
Run 10	40.82	1.15	287.51	7	524.7
Run 12	54.42	0.77	143.75	2.72	543.28
Run 13	54.42	1.15	287.51	2.28	543.28

Table 2 Material properties of Liquid and Vapour phases in various pressures

Pressure (atm)	Phase	Density (kg/m3)	Viscosity (Pa.s)	Thermal Conductivity (W/m-K)	C_p (j/kg-K)	Enthalpy (kJ/kg)	Surface Tension (n/m)	T_{sat} (K)
13.6	Liquid	871.9	0.0,001,389	0.6668	4464.6	824	0.038,964	466.86
	Vapour	6.9105	1.55×10^{-5}	0.03,892	2896.4	27787.9		
20.4	Liquid	847.7	0.00,012,505	0.65,411	4576	916.23	0.034,441	487.22
	Vapour	10.375	1.62×10^{-5}	0.042,921	3220.7	2799		
27.2	Liquid	828.17	0.00,011,638	0.642	4681.5	986.5	0.03,092	502.37
	Vapour	13.786	1.67×10^{-5}	0.046,197	3511.9	2802.8		
40.8	Liquid	796.58	0.00,010,541	0.61,942	4886.9	1093.3	0.025,492	524.7
	Vapour	20.512	1.76×10^{-5}	0.051,676	4053.8	2800.4		
54.4	Liquid	767.24	9.74×10^{-5}	0.59,573	5125	1185.9	0.021,306	543.28
	Vapour	28.135	1.83×10^{-5}	0.057,154	4661.3	27789.6		

For achieving y^+ value of less than 5 on the wall (k-ω SST requirement), a mesh inflation coefficient was initially defined on the wall and corrected adaptively for every 100 iterations depending on the flow conditions during computation process. In adopting mesh size required for y^+ limit on the wall, cell aspect ratios were checked to avoid any large magnitudes. The maximum aspect ratio over all cases was recorded to be 4.38. For executing this coupled Eulerian multi-phase model with high mesh refinement and submodels calculating heat partitions, parallel computing having 16 computational cores was deployed.

Boundary conditions are set according to experimental assumptions and common numerical restrictions. Fully developed profiles for velocity and turbulence characteristics, for liquid phase are calculated through sufficient straight length (with the given cross section), and applied on the inlet boundary where vapour fraction is zero and liquid temperature is set with reference of subcooling temperatures. Outlet boundary is adjusted as pressure outlet with zero gauge back pressure and all the external walls are considered as adiabatic which forces all the generated heat to flow through solid-fluid interface. Heat generation rate (heat flux) is distributed in the solid zone with two forms of uniform or non-uniform as it is explained in the validation section to match with experimental assumptions.

(iii) Heat partitioning scheme

In this fully nucleate boiling regime, the evaporation and quenching heat flux components do remain the dominating terms for most areas of the channel. On the other hand at sharp corners of the channel, the vapour heat flux begins to become comparable with the evaporative and quenching terms, indicating the relative importance of vapour diffusion. This effect is much more prominent when the wall heating is increased and the flow boiling approaches dry-out conditions. Therefore this fourth (vapour heat flux) heat partitioning component will be essential for the model to be comprehensive.

(iv) Momentum exchange and Drag scheme

In the Eulerian scheme, the momentum exchange term is the strongest interfacial parameter coupling momentum conservation equations of phases. As indicated by Eqs. (22–25), this interfacial parameter is heavily dependent on the drag force along with particulate relaxation time and bubble diameter. Therefore, the selection of appropriate drag coefficient in accordance with the boiling flow regime is crucial for precise modelling of convective boiling process. In addition, the slip velocity between phases is also a parameter affecting phase momentum exchange while being dependent on the overall mixture velocity and the liquid evaporation rate.

As mentioned earlier, almost all published boiling models assume bubbly flow and incorporates a single drag coefficient to estimate drag from continuous liquid phase on bubbles as dispersed phase. This approach breaks down as the void fraction is increased as the multi-phase regime no longer remains purely bubbly flow. This modelling weakness is overcome in the current work by modifying the

drag coefficient depending on the boiling flow regime through Eq. (24). This is demonstrated in Fig. 4 using the test data from Pierre and Bankof [41].

Pierre and Bankof [41] measured the radially averaged velocity of each phase $(\bar{v}_v = \bar{\alpha}_v G_v / A_c)$ and calculated the corresponding mixture velocity $\bar{v}_m = \bar{\alpha}_v.\bar{v}_v + (1 - \bar{\alpha}_v).\bar{v}_l$ to correlate slip velocity for the range of operational conditions given in Table 1. For these identical test conditions, predicted vapour (gas) and mixture velocities were obtained from the current model with the modified drag scheme, which accounts for bubbly ($\alpha_v < 0.4$) or mist ($\alpha_v > 0.8$) or churn turbulent regimes. To further ascertain the effectiveness of the proposed drag scheme, (gas) and mixture velocities were also computed using only the traditional approach of bubbly flow scheme. As a plot of gas velocity against mixture velocity, Fig. 4a compares the predicted velocities using the pure bubbly flow assumption (red symbols) with Pierre and Bankof [23, 41] results (black symbols) given in Table 1. Similarly, Fig. 4b provides a comparison between predicted results using the proposed new drag scheme (blue symbols) and Pierre and Bankof [23, 41] results.
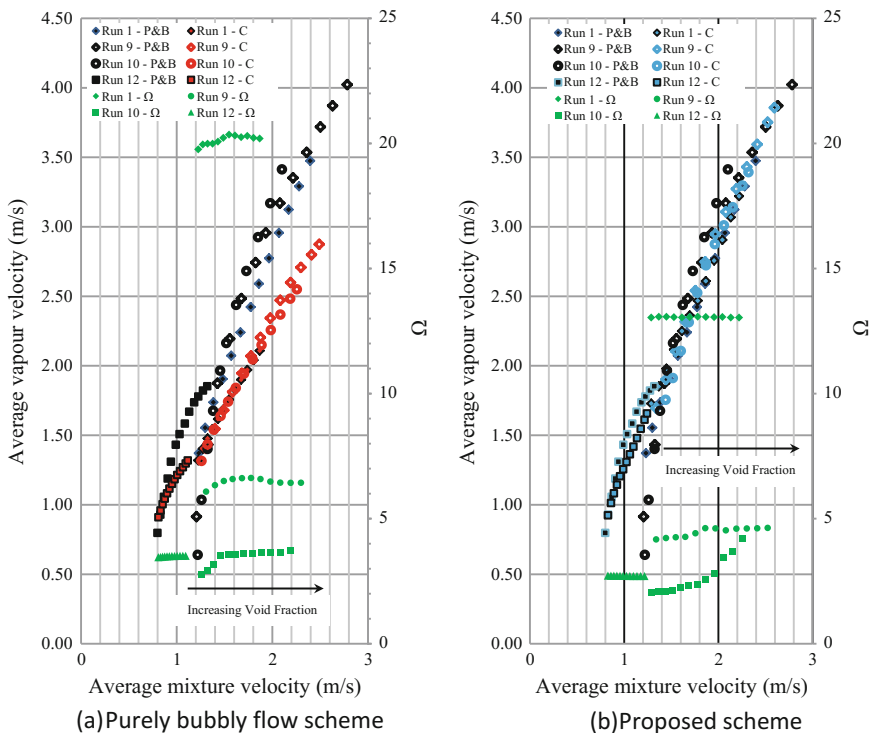

Fig. 4 Comparison of gas velocity and dimensionless wall temperature for bubbly and proposed drag schemes—P&B (Pierre and Bankof), C (Current work) (*Black symbols* represent experimental values from Pierre and Bankof [23, 41])

Figure 4a clearly shows that the predicted results using the bubbly flow scheme deviate significantly from the experimental data with increasing void fraction while continually underestimating the values. To the contrary as illustrated in Fig. 4b, the current scheme highly improves data matching in values and trends with the experimental data consistently over the entire test range. This is a clear indication of the effectiveness in using the proposed multi-tiered drag scheme for accurate representation of convective boiling within all regimes from bubbly to mist flows.

Phase velocity is envisaged to have direct influence on the heat transfer rates within liquid and vapour phases and indirectly affecting the evaporative heat flux. To demonstrate this thermal dependency, a dimensionless temperature term Ω is defined as $\Omega = \frac{T_w - T_{in}}{T_{Sat} - T_{in}}$ and included in Fig. 4 (green symbols) for both drag schemes. Comparison indicates up to 54% difference in Ω (representing up to 7° difference in wall superheat) between schemes and a higher dependency on scheme for large void fractions. Accordingly, the improvement of drag scheme could be interpreted as equally being significant for the accuracy of liquid and vapour convective heat fluxes in the proposed partitioning approach.

(v) Bubble departure frequency and quenching correction

Process of vapour bubble generation is essential for a time-averaged convective boiling model in estimating wall heat flux components due to quenching and evaporation, expressed by Eq. (18.a, 18.b). Between two successive bubble departures at a nucleation site, bubble formation is divided into two stages known as periods of bubble dwelling (waiting) and growth of which the total duration determines the bubble departure frequency.

In the dwelling phase, a bubble resides within a cavity and develops in size to reach cavity mouth. Heat conduction from the wall to liquid during this phase accounts for the quenching heat flux defined by Eq. (18.a). In subsequent growth period, a bubble undergoes much rapid development outside the cavity attached to the wall surface until its detachment. During this phase, bubble removes heat from the surface by evaporation defined as evaporative heat flux in Eq. (18.b).

In determining bubble departure frequency, a correlation developed by Cole [13] is traditionally used in boiling models. This is originally derived for pool boiling and estimates the overall time period between two consecutive bubble departures, hence the detachment frequency. However, this model does not separate individual time periods for dwelling and growth phases. In addition, Cole [13] formulated this departure model treating buoyancy to be the key driving mechanism for bubble detachment. Nonetheless in convective boiling, both buoyancy and inertial (shear-induced) forces are essentially involved in bubble departure mechanism. Consequently, the Cole model is thought to be inadequate for convective boiling.

To evaluate the relative influence from inertial force and surface tension, the current model makes use of Weber number (We) (inertial to surface tension ratio), where We towards 1 indicates inertia dominance while We toward 0 signifies surface tension control. For this, surface Weber number $\left(We_s = \frac{\rho D_h u_*^2}{\sigma} \right)$ is defined with respect to frictional velocity of liquid phase on the heated surface (u_*) and duct

hydraulic diameter (D_h). This is then used for appraising the applicability of available bubble detachment models.

Podowski [16] and Basu [15] models accounted for buoyancy and inertial (shear-induced) forces and are potentially considered for convective boiling. However, Basu [15] formulation requires prior knowledge of contact angle values (on the surface) whilst Podowski does not depend on such additional uncertainties. In the current simulation, Podowski model is deployed, supported by its additional analytical advantages.

Podowski model quantifies bubble dwelling and growth times separately whereby it warrants accurate determination of quenching heat flux at the heated wall. Recalling Eq. (18.a), the quenching heat flux is computed by integrating over the bubble cycle period $\tau_{B-Cycle}$. With Cole model, $\tau_{B-Cycle}$ is compelled to assume as the time duration between consecutive bubble detachments. This is inaccurate since wall the quenching process only occurs during the dwelling stage followed by evaporation over the bubble cycle. To account for this in the current scheme, the total duration of bubble cycle $\tau_{B-Cycle}$ is split into dwelling (τ_D) and growth (τ_G) times. Then, a time correction factor defined by $\sqrt{\frac{\tau_D}{\tau_D + \tau_G}}$ is applied for quenching heat flux computed from $\tau_{B-Cycle}$. Similarly, the evaporative heat flux is modified accordingly with $\sqrt{\frac{\tau_G}{\tau_D + \tau_G}}$.

Figure 5a shows, the contours of surface Weber number at the fluid-wall interface of the heated duct wherein red regions having $We \approx 1$ represent the inertia dominated high convective flow while blue areas with $We \approx 0$ where surface tension controls flow dynamics. This large variation of We affirms the fact that Podowski [16] approach for bubble departure is more applicable in convective

(a) Surface Weber number (b) Bubble departure frequency (Hz) (c) Profiles along section "A-A"
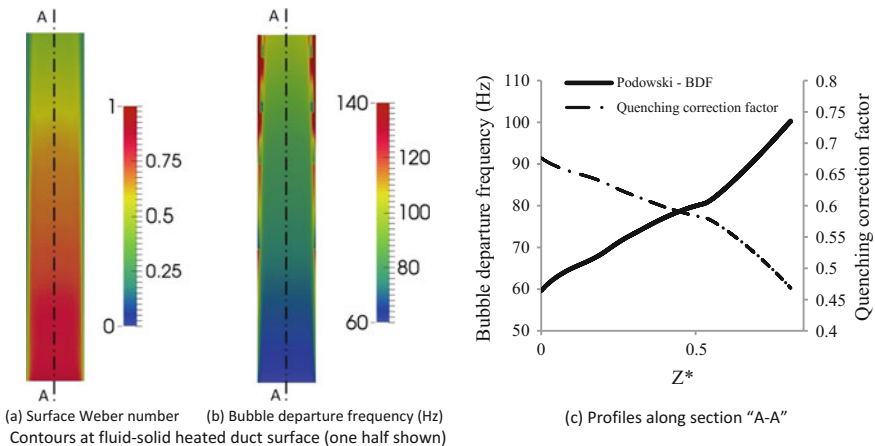Contours at fluid-solid heated duct surface (one half shown)

Fig. 5 Surface Weber number, Bubble departure frequency and quenching correction factor using Podowski scheme with Run 10 (Table 3)

boiling than the Cole [13] model, where that latter would only be meaningful in near-stagnant regions of the flow.

Figure 5b illustrates the distribution of bubble departure frequency based on Podowski approach over the heated duct surface. It clearly shows a wide variation to the bubble departure frequency ranging from low values (blue) to high values (red) in convective flow. Additionally, Fig. 5c depicts the local values of correction factor for quenching heat flux along the section A-A. It shows the trend of reducing dwelling time (or such correction) whilst increasing departure frequency due to inertial effects of convective flow. On the contrary, Cole bubble departure model based on pool boiling would predict indiscriminately a single constant frequency of 145.98 Hz throughout the heated section. Accordingly as a major convective boiling model improvement, Podowski scheme is incorporated into the current boiling simulation, accounting for both inertial and buoyancy forces with correction to quenching and evaporative time scales.

Bubble departure frequency invariably affects the void fraction and bubble nucleation rate. Figure 6 compares the predicted void fraction results obtained by using Cole and Podowski models against the Pierre and Bankof [41] experimental data. The figure indicates that the Cole scheme consistently overpredicts the void fraction because of the overestimation in the bubble departure frequency by this scheme, whereas the Podowski approach is much more compatible with the void fraction date of Pierre and Bankof [41]. This signifies the need to assign appropriate of bubble frequency model in convective boiling simulation analysis.

Quenching heat flux along section "A-A" in Fig. 5, are shown on the secondary axis of Fig. 6. It is evident that the quenching heat flux is underestimated near duct inlet compared to Podowski model owing to the overprediction of evaporative heat flux through bubble mechanism captured in Cole scheme. This observation further establishes effectiveness in Podowski model for convective boiling.

For reference and comparison, Table 3 provides a summary of bubble departure frequency and quenching correction factor for each model in terms of dimensionless temperature.

(vi) Wall lubrication model

Bubbles growing at a heated surface undergo either a process of sliding and then lift-off or rapid lift-off without sliding, depending on the flow conditions. In both of these cases following detachment, bubbles move towards the core (or bulk) flow area where bubble may potentially collapse due to vapour condensation. For this reason in convective boiling, maximum void fraction is expected to occur in vicinity of the heated wall with the presence of a contact liquid layer. This liquid layer offers an interfacial shear effect known as Wall Lubrication Force [Eq. (28)] on the vapour phase, whose influence is significant towards predicting the flow field hydrodynamics, void generation and heat transfer rate.

The influence of lubrication force on the phase pattern and location of maximum vapour vicinity is illustrated in Fig. 7a where void fraction contours at a cross section near duct exit are compared for non-lubricated (NL) and lubricated (L) cases.
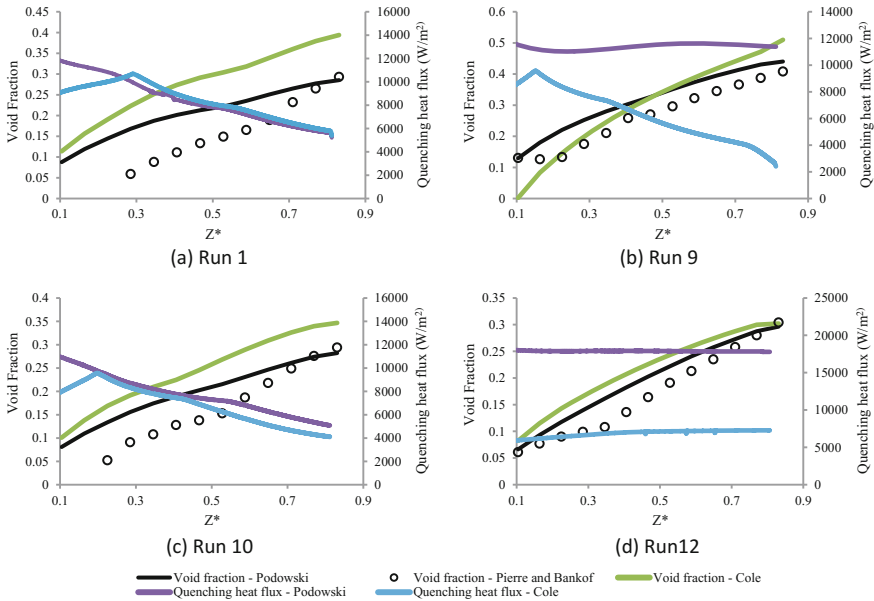
Fig. 6 Variations of void fraction and quenching heat flux along section A-A (Fig. 3)

Table 3 Average bubble departure frequency, quenching correction factor and dimensionless temperature at fluid-solid interface

Run No	Bubble Departure Frequency (Hz)		Quenching Correction Factor		Dimensionless Temperature Ω	
	Cole	Podowski	Cole	Podowski	Cole	Podowski
1	145.46	145.67	–	0.33	9.30	7.58
2 and 3	147.48	62.14	–	0.93	8.34	3.03
4 and 5	146.41	67.91	–	0.91	7.47	2.02
6	143.13	62.71	–	0.88	6.32	1.51
7	146.41	95.45	–	0.91	13.11	5.28
8	147.08	107.86	–	0.25	7.86	2.39
9	145.73	63.46	–	0.44	9.65	2.54
10	145.98	83.35	–	0.32	2.20	1.96
12	144.92	23.96	–	1.00	1.50	1.94
13	145.05	46.37	–	0.93	12.05	2.46

Figure 7b compares radially averaged void fraction and averaged dimensionless temperature over duct cross section with (L) and without (NL) wall lubrication model for Runs 12 and 13. It is observed that the wall temperature is overpredicted in the absence of wall lubrication forces with reduced heat transfer rates through vapour at the wall. This effect is more pronounced for flow with higher void fraction.
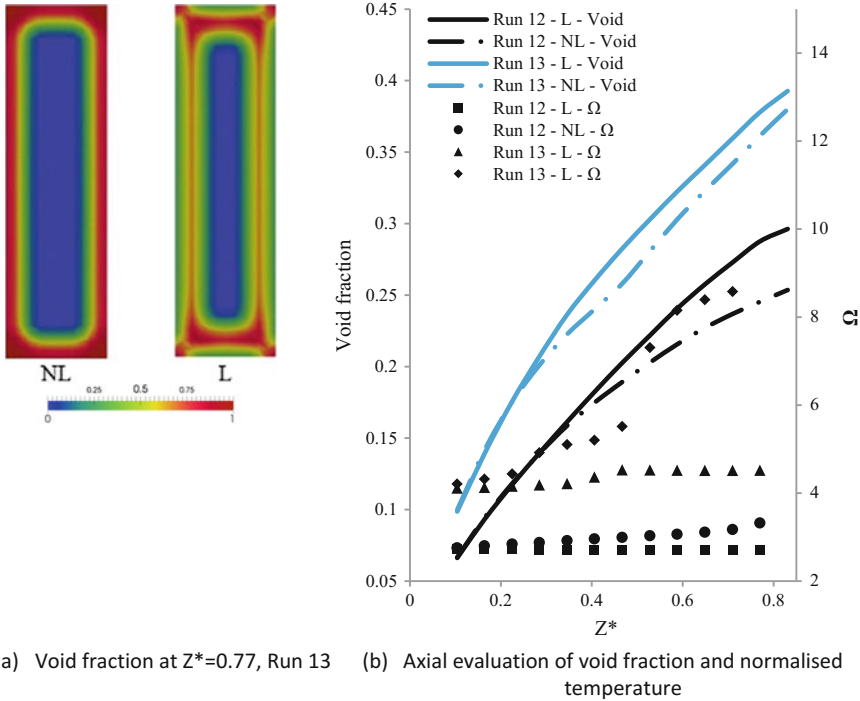
(a) Void fraction at Z*=0.77, Run 13   (b) Axial evaluation of void fraction and normalised temperature

Fig. 7 Influence of lubrication force of phase field and domain parameters

For improved thermal modelling, the current model includes the wall lubrication effect where by wall heat removal occurs as a combination of quenching and evaporation processes. Without this consideration of lubrication forces, the vapour diffusion governs the heat flux component and predicts premature wall liquid layer dry-out, which is unrealistic as the case with existing boiling models.

4 Appraisal of Thermal Benefits and Potential for Energy Saving

Above modelling strategies are proposed to capture the unique characteristics of convective boiling thereby imparting a better physical representation of boiling heat and mass exchange phenomena in the numerical simulation practice. In these, a key contributor is the use of Podowski model [16] in conjunction with a dwelling and growth time modification, instead of the traditional Cole closure [13] approach. The former model is more compliant with thermal and fluid mechanics of convective boiling, for it is built upon wall heat partitioning technique, and accounts for inertia and buoyancy effects imposed by flow fields in the vicinity of bubble interface.

On the other hand, the latter model carries inherent mechanistic weakness as it is specifically developed for pool boiling with no implications from flow fields. Moreover, Cole model does not differentiate the significance of dwelling and growth phases of bubble life in evaluating wall heat flux-it computes both quenching and evaporative heat fluxes by considering the entire bubble life or departure time, hence grossly over-estimating these heat components. Such predictive inaccuracies are translated into and reflected as non-optimal system design, energy and resource wastage, and poor overall plant thermal efficiency. Also, inadequately designed systems may experience operating instabilities and load fluctuations.

The proposed modelling strategy uses the Podowski model and integrates appropriately weighted dwelling time (quenching) and growth time (evaporative), to refine quenching and evaporative wall heat flow components. Furthermore, it incorporates wall lubrication and turbulence models, which are not considered in the current boiling simulation methodologies. Consequently, these modelling refinements permit precise capturing of convective boiling characteristics beyond the realms of current practice limited to low void fraction boiling and extending the applicability from bubbly flow towards annular flow, where void fraction is much larger. Resulting degree of modelling enhancements and energy-saving potential are clearly evident from Fig. 8, where local boiling wall heat fluxes along the pipe are illustrated and compared for identical simulations using Podowski and Cole models, separately. In this, Run 1 and Run 12 test conditions given in Tables 1 and 2 are used for the comparison, covering both low and high void fraction flow conditions in convective boiling.

In Fig. 8, the results for Cole model clearly show a consistent overestimation of wall heat flux by about 19% over the Podowski model for Run 1 and 35% for Run 2, that arise from the reasons explained above. This is indicative of the
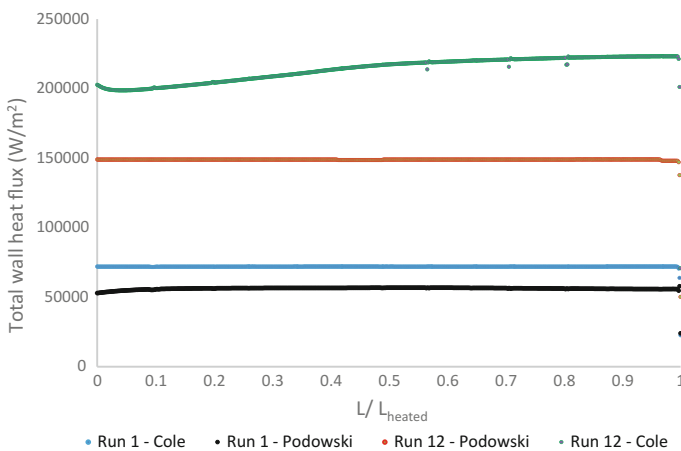

Fig. 8 Local wall heat flux estimated by Cole and Posowski bubble departure frequency models

energy-saving potential and resource utilisation efficiency brought about by the use of proposed enhancement strategies, allowing the application of much stringent parametric and thermal energy estimations leading to improved overall boiling system design.

5 Conclusions

Review of reported literature indicates significant weaknesses in the published CFD simulation models for convective boiling. Contributing to model enhancement, this book chapter presents a numerical study introducing modifications to bubble dynamics and momentum exchange closures while adopting enhanced modelling elements that were not previously considered or included. The suggested framework could be referenced as a comprehensive modelling approach for internal convective boiling within pipe systems.

These contributions are summarised below:

- Based on Eulerian framework, the study developed a modified methodology for capturing momentum transfer between phases undergoing vapour–liquid phase change. In this, framework of primary and secondary phases was modified and a tiered approach was included for the local drag coefficient to improve the applicability of the analysis from bubbly regime (low void fraction) to mist regime (high void fraction). These improvements were very tangibly noticed in reducing results over prediction, particularly in void fraction, that consistently prevalent in previous convective boiling models. Consequently, the study identified that the slip velocity between phases play, although indirectly, a pivotal role in interfacial properties exchange and convective boiling heat and mass transfer.
- Current model incorporates Podowski [16] approach for accurate determination of bubble departure frequency by accounting for dwelling and growth periods. This methodology significantly improved estimations of quenching and evaporative heat fluxes associated with bubble growth. The predicted results showed improved agreement with experimental data over all boiling regimes and were observed to be much more accurate than the traditional Cole [11] correlation extensively used in previous studies.
- The study identifies critical modelling elements that were not previously included in numerical analysis of convective boiling. These include wall lubrication force and additional turbulence modelling compliances both of which were shown to improve validation and enhanced overall simulation approach for convective boiling with high void fraction.
- The proposed simulation enhancement strategies are shown to be very proficient towards accurate estimation of convective boiling design parameters leading to much improved overall thermal system design and resource utilisation, with significant technical contributions towards a sustainable energy future.

References

1. Collier, J. G. (1972). Convective Boiling and Condensation. McGraw-Hill book Company (UK). Second edition.
2. Lockhart, R. W., & Martinelli, R. C. (1949). Proposed correlation of data for isothermal two-phase two-component flow in pipes. Chem eng prog. 45.
3. Martinelli, R. C., & Nelson, D. B. (1948). Prediction of pressure drop during forced circulation boiling of water. *Tran Journal ASME, 70,* 695.
4. Zuber, N., & Findaly, J. (1965). Average Volumetric Concentration in two-phase flow systems. *Trans ASME Journal of Heat Transfer, 87,* 453.
5. Bangkof, S. G. (1960). A variable density single-fluid model of two-phase model with particular reference to water-vapour flow, Trans ASME. J. Heat Trans. Series C.82.
6. Marchaterre, J. F., & Hoglund, B. W. (1962). Correlation for two-phase flow. *Nucleonic, 142.*
7. Griffith, P. (1963). The slug-annular flow regime transition at elevated pressure. ANL-6796.
8. Bergles, A. E., & Rohesnow, W. M. (1964). The determination of forced-convection surface-boiling heat transfer. *ASME. Journal Heat Transfer, 86,* 365–372.
9. Kandlikar, S. G. (1990). A general correlation for saturated two-phase flow boiling heat transfer inside horizontal and vertical tubes. *ASME. Journal Heat Transfer, 112,* 219–228.
10. Boyd, R. D., & Meng, X. (1995). Boiling curve correlation for subcooled flow boiling. *International Journal Heat and Mass Transfer, 38–4,* 758–760.
11. Cole, R. (1960). A photographic study of pool boiling in the region of the critical heat flux. *AIChE Journal, 6–4,* 533–538.
12. Thorncroft, G. E., Klausnera, J. F., & Mei, R. (1998). An experimental investigation of bubble growth and detachment in vertical up-flow and down-flow boiling. *International Journal Heat and Mass Transfer, 41,* 3854–3871.
13. Situ, R., Mi, Y., Ishii, M., & Mori, M. (2004). Photographic study of bubble behaviours in forced convection subcooled boiling. *International Journal Heat and Mass Transfer, 47,* 3659–3667.
14. Situ, R., Hibiki, T., Ishii, M., & Mori, M. (2005). Bubble lift-off size in forced convective subcooled boiling flow. *International Journal Heat and Mass Transfer, 48,* 5536–5548.
15. Basu, N., Warrier, G. R., & Dhir, V. K. (2005). Wall heat flux partitioning during subcooled flow foiling: part 1—model development. *ASME Joural Heat Transfer, 127,* 131–140.
16. Podowski, R. M., Drew, D. A., Lahey, R. T., Podowski, J. R., & M.Z. (1997). A mechanistic model of ebullition cycle in forced convection sub-cooled boiling. In: *Proceeding of the 8th International topical meeting on nuclear reactor thermal hydraulic.* Kyoto, Japan. vol. 3.
17. Situ, R., Ishii, M., Hibiki, T., Tu, J. Y., Yeoh, G. H., & Mori, M. (2008). Bubble departure frequency in forced convective subcooled boiling flow. *International Journal Heat and Mass Transfer, 51,* 6268–6282.
18. Kurul, N., & Podowski, M. Z. (1990). Multidimensional effects in forced convection Subcooled Boiling. In: *9th International Heat Trans Conference.* Jerusalem. Israel, Proceedings.
19. Koncar, B., Kljenak, I., & Mavko, B. (2004). Modelling of local two-phase flow parameters in upward subcooled flow boiling at low pressure. *International Journal Heat and Mass Transfer, 47,* 1499–1513.
20. Krepper, E., Koncar, B., & Egorov, Y. (2007). CFD modelling of subcooled boiling-Concept, validation and application to fuel assembly design. *Nuclear Engineering and Design, 237,* 716–731.
21. Koncar, B., & Krepper, E. (2008). CFD simulation of convective flow boiling of refrigerant in a vertical annulus. *Nuclear Engineering and Design, 238,* 693–706.
22. Abishek, S., Narayanaswamy, R., & Narayanan, V. (2013). Effect of heater size and Reynolds number on the partitioning of surface heat flux in subcooled jet impingement boiling. *International Journal Heat and Mass Transfer, 59,* 247–261.

23. Pierre, C. C. S. T., & Bankoff, S. G. (1967). Vapour volume profiles in developing two-phase flow. *International Journal Heat and Mass Transfer, 10,* 237–249.
24. Menter, F. R. (2009). Review of the SST turbulence model experience from an industrial perspective, Int. *Journal Computational Fluid Dynamics, 23–4,* 305–316.
25. Inc, A. N. S. Y. S. (2012). ANSYS FLUENT theory guide. *Release, 14,* 5.
26. Troshko, A. A., & Hassan, Y. A. (2001). A two-equation turbulence model of turbulent bubbly flows. *International Journal Multi-phase Flow, 27,* 1965–2000.
27. Sato, Y., & Sadatomi, M. (1981). Momentum and heat transfer in two-phase bubble flow—I. Theory. *International Journal Multiphase Flow, 7–2,* 167–177.
28. Sato, Y., & Sekoguch, K. (1975). Liquid velocity distribution in two-phase bubble flow. *International Journal Multiphase Flow, 2–1,* 79–95.
29. Lavieville, J., Quemerais, E., Mimouni, S., Boucker, M., & Mechitoua, N. (2005). NEPTUNE CFD V1.0 Theory Manual, EDF.
30. Del Valle M, V. H., & Kenning, D. B. R. (1985). Subcooled flow boiling at high heat flux. International Journal Heat and Mass Transfer *28,* 1907–1920.
31. Lemmert, M., & Chawla, L. M. (1977). *Influence of flow velocity on surface boiling heat transfer coefficient in Heat Transfer in boiling*. NY, USA: Academic Press and Hemisphere.
32. Tolubinski, V. I., & Kostanchuk, D. M. (1970). Vapour bubbles growth rate and heat transfer intensity at subcooled water boiling. In: *4th International Heat Transfer Conference*, Paris, France. Proceeding.
33. Apte, S. V., Gorokhovski, M., & Moin, P. (2003). LES of atomizing spray with stochastic modelling of secondary breakup. *International Journal Multiphase Flow, 29,* 1503–1522.
34. Unal, H. C. (1979). Maximum Bubble diameter, maximum bubble growth time and bubble growth rate during subcooled nucleate flow boiling of water up to 17.7MN/m2. *International Journal Heat and Mass Transfer, 19,* 643–649.
35. Kataoka, I., Ishii, M., & Mishima, K. (1983). Generation and size distribution of droplet in annular two-phase flow. *ASME Journal Fluid Engineering, 105,* 230–238.
36. Ishii, M., & Zuber, N. (1979). Drag coefficient and relative velocity in bubbly, droplet or particulate flows. *AlChE Journal, 25–5,* 843–855.
37. Moraga, F. J., Bonetto, F. J., & Lahey, R. T. (1999). Lateral forces on spheres in turbulent uniform shear flow. *International Journal Multiphase Flow, 25,* 1321–1372.
38. De Bertodano, M. L. (1991). Turbulent bubbly flow in a triangular duct. Ph.D. Thesis, Rensselaer Polytechnic Institute, New York.
39. Hosokawa, S., Tomiyama, A., Misaki, S., & Hamada, T. (2002). Lateral migration of single bubbles due to the presence of wall. In: *ASME Joint U.S.-European Fluids Engineering Division Conference*, Montreal, Canada.
40. Ranz, W. E., & Marshall, W. R. (1952). Evaporation from drops. *Parts I & II. Chemical Engineering, 48*(141–6), 173–180.
41. Pierre, C. C. S. T. (1965). Frequency-Response analysis of steam voids to sinusoidal power modulation in a thin-walled boiling water coolant channel, Arogan National Labratoary, ANL-7041.
42. Lemmon, E. W., McLinden, M. O., & Friend, D. G., (2013). Thermophysical Properties of Fluid Systems, NIST Chemistry WebBook, NIST Standard Reference Database Number 69, National Institute of Standards and Technology, Gaithersburg MD, 20899. http://webbook.nist.gov.